Dalton Transactions

ROYAL SOCIETY OF CHEMISTRY

PAPER

View Article Online
View Journal | View Issue



Cite this: *Dalton Trans.*, 2025, **54**, 7115

# Copper(II) complexes with (*E*)-4-(2-(pyridin-2-ylmethylene)hydrazinyl)quinazoline and non-steroidal anti-inflammatory drugs: structure and biological evaluation†

Chrisoula Kakoulidou, Antonios G. Hatzidimitriou and George Psomas *

Received 21st February 2025,
Accepted 27th March 2025

DOI: 10.1039/d5dt00435g

rsc.li/dalton

Four novel Cu(II) mixed-ligand complexes containing the quinazoline (*E*)-4-(2-((pyridin-2-yl)methylene) hydrazinyl)quinazoline (HL) or its methoxylated derivative ($HL^1$) and a non-steroidal anti-inflammatory drug (mefenamic acid, flufenamic acid, diflunisal or diclofenac) as ligands were synthesized and characterized using single-crystal X-ray crystallography. In these complexes, the quinazolines act as tridentate or bridging tetradentate ligands. The studied biological properties of these complexes included the interaction with calf-thymus DNA, the ability to cleave supercoiled circular pBR322 plasmid DNA in the absence or presence of irradiation of various wavelengths, the ability to reduce $H_2O_2$ or to scavenge free radicals such as 1,1-diphenyl-picrylhydrazyl and 2,2′-azino-bis-(3-ethylbenzothiazoline-6-sulfonic acid), and the affinity for bovine serum albumin. These compounds can bind tightly to calf-thymus DNA *via* intercalation, and most of them induce notable (photo)cleavage of plasmid DNA. They can also bind tightly and reversibly to albumin and exhibit moderate-to-significant activity towards 2,2′-azino-bis-(3-ethylbenzothiazoline-6-sulfonic acid) radicals and $H_2O_2$.



## 1 Introduction

Being the third most abundant trace element in the human body,[1] copper plays a crucial *in vitro* role by participating in the active center of many enzymes, such as Cu–Zn superoxide dismutase, contributing thus to the protection from oxidative damage in biological species.[1,2] As a result of its biological activity, copper is used as a bacteriostatic material in knobs and contact surfaces in hospitals[3] and is present in medicaments such as CuAlgesal® (used for the treatment of arthritis) or Casiopeinas® (in clinical trials for anticancer activity).[4,5] Recent literature reports revealed Cu(II) complexes with promising *in vitro* biological activities.[6–8]

4-Quinazoline-hydrazones are compounds containing two scaffolds known for more than a century:[9] quinazoline with two fused aromatic (benzene and pyrimidine) rings[10] and noteworthy biological properties,[11,12] and hydrazone with the characteristic imine group[13] and significant biological and catalytic activities.[14–16] Within this context, 4-quinazoline-hydrazones are considered hybrid molecules combining the structural features of both quinazolines and hydrazones in order to enhance or differentiate their activities. In particular, there are reports regarding 4-quinazoline-hydrazone derivatives with noteworthy antiproliferative efficacy[17] or phosphodiesterase inhibitory activity[18] and their metal complexes with interesting photophysical properties.[18,19]

Non-steroidal anti-inflammatory drugs (NSAIDs) are analgesic and anti-inflammatory drugs used to treat symptoms, pain and inflammation originating from injuries and/or diseases.[20,21] NSAIDs are co-administered with anticancer drugs[22] and exhibit cytotoxic activity *via* apoptosis[23] or radical scavenging.[24] The NSAIDs used in the present research are the salicylate derivative diflunisal (Hdifl), phenylalkanoic acid sodium diclofenac (Na dicl), and the fenamates mefenamic acid (Hmef) and flufenamic acid (Hfluf) (Fig. 1). As typical and commonly used NSAIDs, they were proposed to treat the symptoms of COVID-19 disease,[25] besides their administration in cases of migraine and acute pain (Hmef),[26] moderate dysmenorrhea pain (Hfluf),[27] rheumatoid arthritis (Na dicl),[28] oral surgeries[29] and transthyretin amyloidosis cardiomyopathy (Hdifl).[30]

Combining our previous research projects regarding metal complexes of (*E*)-4-(2-((pyridin-2-yl)methylene)hydrazinyl)quinazoline (HL, Fig. 2) and its halogenated derivatives,[31–34] as well as copper(II) complexes with NSAIDs,[21,35–40] we have syn-

*Department of General and Inorganic Chemistry, Faculty of Chemistry, Aristotle University of Thessaloniki, GR-54124 Thessaloniki, Greece.*
*E-mail: gepsomas@chem.auth.gr*

† Electronic supplementary information (ESI) available. CCDC 2418543–2418546. For ESI and crystallographic data in CIF or other electronic format, see DOI: https://doi.org/10.1039/d5dt00435g

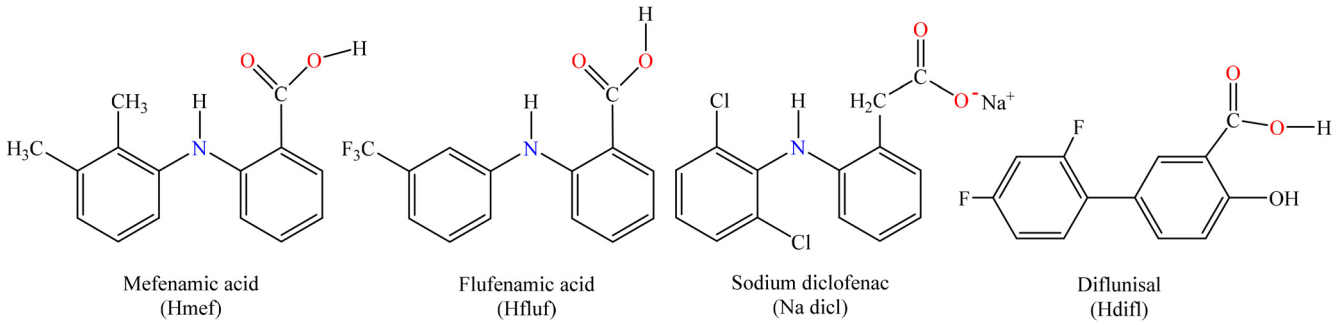


**Fig. 1** The syntax formula of the NSAIDs used in the present study: mefenamic acid (Hmef), flufenamic acid (Hfluf), sodium diclofenac (Na dicl), and diflunisal (Hdifl).

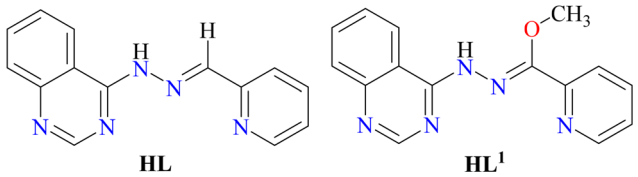


**Fig. 2** The syntax formula of HL and its methoxy derivative $HL^1$.

thesized and characterized four novel hybrid Cu(II) complexes containing a quinazoline (HL or its methoxy derivative $HL^1$) and an NSAID (Hdifl, Hmef, Na dicl or Hfluf, Fig. 1). The characterization of the complexes was performed using spectroscopic techniques (IR, UV-vis) and single-crystal X-ray crystallography. The novel complexes were examined *in vitro* regarding their (i) interaction with calf-thymus (CT) DNA and competition with ethidium bromide (EB) with the aim of calculating the DNA-interaction mode and DNA-binding, (ii) ability to cleave supercoiled circular pBR322 plasmid DNA (pDNA) and the effect of UVA, UVB or visible light on cleavage ability, (iii) ability to reduce $H_2O_2$ and to scavenge free radicals, such as 1,1-diphenyl-picrylhydrazyl (DPPH) and 2,2′-azino-bis-(3-ethylbenzothiazoline-6-sulfonic acid) (ABTS), and (iv) affinity for bovine serum albumin (BSA) (with the purpose of calculating the binding constant and determine the binding site).

# 2 Experimental

## 2.1 Materials – instrumentation – physical measurements

All chemicals and solvents were of reagent grade and were used as purchased from commercial sources: $CuCl_2{\cdot}2H_2O$, Hfluf, Hmef, CT DNA, EB, BSA, ABTS, $K_2S_2O_8$, nordihydroguaiaretic acid (NDGA), and butylated hydroxytoluene (BHT) were from Sigma-Aldrich Co.; 6-hydroxy-2,5,7,8-tetramethylchromane-2-carboxylic acid (Trolox) was from J&K; Na dicl, sodium warfarin, ibuprofen, and DPPH were from TCI; Hdifl was from Fluka; trisodium citrate dihydrate, NaCl, and $NaH_2PO_4$ were from Merck; Tris base, boric acid, EDTA disodium salt dehydrate, loading buffer and $H_2O_2$ (30% w/v) were from PanReac Applichem; supercoiled circular pBR322 plasmid DNA was from New England Bioline; and L-ascorbic acid and all solvents were from Chemlab.

The CT DNA stock solution was prepared by the dilution of CT DNA to buffer (containing 150 mM NaCl and 15 mM trisodium citrate at pH 7.0) followed by exhaustive stirring at 4 °C for 2 days and was kept at 4 °C for a week. The stock solution of CT DNA gave a ratio of UV absorbance at 260 and 280 nm ($A_{260}/A_{280}$) of ~1.88, indicating that the DNA was sufficiently free from protein contamination.[41] The DNA concentration per nucleotide was determined by the UV absorbance at 260 nm after a 1 : 20 dilution using $\varepsilon = 6600\ M^{-1}\ cm^{-1}$.[42]

Infrared (IR) spectra (400–4000 $cm^{-1}$) were recorded on a Nicolet FT-IR 6700 spectrometer with samples prepared as KBr pellets (abbreviations used: br = broad, m = medium, s = strong, vs = very strong, w = weak, and $\Delta\nu(COO) = \nu_{asym}(COO) - \nu_{sym}(COO)$). UV-visible (UV-vis) spectra were recorded in solution at concentrations in the range of 5 mM–50 μM on a Hitachi U-2001 dual-beam spectrophotometer. C, H and N elemental analyses were carried out on a PerkinElmer 240B elemental analyzer. Molar conductivity measurements were carried out in 1 mM DMSO solution of the complexes using a Crison Basic 30 conductometer. Fluorescence spectra were recorded in solution with a Hitachi F-7000 fluorescence spectrophotometer. Viscosity experiments were carried out using an ALPHA L Fungilab rotational viscometer equipped with an 18 mL LCP spindle and the measurements were performed at 100 rpm.

## 2.2 Synthesis of the compounds

**2.2.1 Synthesis of ligand HL.** The synthesis of HL was accomplished in three steps including the synthesis of the 4-aminoquinazoline and quinazolin-4-yl-hydrazine as intermediates according to the procedure previously reported.[31]

**2.2.2 Synthesis of complex {[Cu(HL¹)(μ-Cl)](difl)}$_n$ (complex 1).** A methanolic solution of KOH (9 mg, 0.16 mmol) was added into a methanolic solution (~10 mL) of diflunisal (40 mg, 0.16 mmol) and the solution was stirred for 1 h. Afterwards, the solution was added simultaneously with a methanolic solution (~8 mL) of HL (20 mg, 0.08 mmol) to a methanolic solution of $CuCl_2{\cdot}2H_2O$ (14 mg, 0.08 mmol). The reaction solution was stirred for 30 min. After removing the

 

precipitate formed during the cooling process by filtration, the solution was left for slow evaporation at room temperature. After seven days, green single-crystals of complex **1** (25 mg, 50%) suitable for X-ray structure determination were deposited and collected by filtration. Elemental analysis: calcd for [Cu(HL$^1$)(μ-Cl)](difl) ($C_{28}H_{19}ClCuF_2N_5O_4$, MW = 626.48): C 53.68, H 3.06, N 11.18; found: C 53.55, H 3.24, N 10.90%. IR (KBr disk), $\nu$ (in cm$^{-1}$): $\nu$(C═N): 1634(s); $\nu_{asym}$(COO): 1600 (s); $\nu_{sym}$(COO): 1419 (m); $\Delta\nu$(COO) = 181; w(N–H): 764 (s); $\nu$(Cu–N): 526 (m). UV-vis in Nujol, $\lambda$ (in nm): 665, 460, 435. UV-vis in DMSO, $\lambda$ (in nm) ($\varepsilon$, in M$^{-1}$ cm$^{-1}$): 661 (90), 457(sh) (9600), 424 (7980), 395 (sh) (8100), 372 (sh) (5720), 309 (sh) (11 520). The complex is soluble in DMSO ($\Lambda_M$ = 17 mho cm$^2$ mol$^{-1}$, 1 mM DMSO).

**2.2.3 Synthesis of complex [Cu(L)(mef)(CH$_3$OH)]·CH$_3$OH (complex 2).** Complex **2** was prepared in two steps. In the first step, complex [Cu(mef)$_2$(H$_2$O)$_2$] was synthesized according to a previously reported procedure.[39] In the second step, a warm methanolic solution of HL (14 mg, 0.057 mmol) was added dropwise into a methanolic solution (18 mL) of [Cu(mef)$_2$(H$_2$O)$_2$] (33 mg, 0.057 mmol) and the mixture was stirred for 30 min. The reaction mixture was cooled at room temperature and the formed brown precipitate was filtered. The resultant solution was left for slow evaporation and red–brown single-crystals of complex **2** (20 mg, 56%) suitable for X-ray structure determination were deposited after two days and collected by filtration. Elemental analysis: calcd for [Cu(L)(mef)(CH$_3$OH)]·CH$_3$OH ($C_{31}H_{32}CuN_6O_4$, MW = 616.18): C 60.43, H 5.23, N 13.64; found: C 60.58, H 5.04, N 13.43%. IR (KBr disk), $\nu$ (cm$^{-1}$): $\nu$(N–H)$_{secondary}$: 3300 (w); $\nu$(C═N): 1613 (s), 1577 (vs); $\nu_{asym}$(COO): 1595 (s); $\nu_{sym}$(COO): 1381(w); $\Delta\nu$(COO) = 214; $\nu$(Cu–N): 520 (m). UV-vis in Nujol, $\lambda$ (in nm): 640 (sh), 470, 435(sh). UV-vis in DMSO, $\lambda$ (nm) ($\varepsilon$, M$^{-1}$ cm$^{-1}$): 645 (sh) (30), 466 (6500), 440 (sh) (4500), 339 (sh) (3200), 294 (6400). The complex is soluble in DMSO, DMF and THF ($\Lambda_M$ = 2 mho cm$^2$ mol$^{-1}$, 1 mM DMSO).

**2.2.4 Synthesis of complex [Cu(L)(dicl)]$_n$ (complex 3).** A warm methanolic solution (5 mL) of HL (30 mg, 0.12 mmol) and a warm methanolic solution (7 mL) of sodium diclofenac (39 mg, 0.12 mmol) were added simultaneously in a methanolic solution (3 mL) of CuCl$_2$·2H$_2$O (21 mg, 0.12 mmol). The brown precipitate initially formed was removed by filtration. The resultant solution was layered with diethyl ether and was left to evaporate slowly at room temperature. Brown single-crystals of complex **3** (25 mg, 35%) suitable for X-ray structure determination were collected after two days. Elemental analysis: calcd for [Cu(L)(dicl)] ($C_{28}H_{20}Cl_2CuN_6O_2$, MW = 606.96): C 55.41, H 3.32, N 13.85; found: C 55.25, H 3.47, N 13.60%. IR (KBr disk), $\nu$ (in cm$^{-1}$): $\nu$(C═N): 1613 (m); $\nu_{asym}$(COO): 1575 (m); $\nu_{sym}$(COO): 1359 (w); $\Delta\nu$(COO) = 216; (Cu–N): 525 (m). UV-vis in Nujol, $\lambda$ (in nm): 690 (sh), 465, 437 (sh). UV-vis in DMSO, $\lambda$ (in nm) ($\varepsilon$, in M$^{-1}$ cm$^{-1}$): 695 (sh) (95), 464 (19 500), 439 (sh) (17 080), 279 (23 620). The complex is soluble in DMSO ($\Lambda_M$ = 4 mho cm$^2$ mol$^{-1}$, 1 mM DMSO).

**2.2.5 Synthesis of complex [Cu$_4$(L$^1$)$_2$(fluf)$_4$(Cl)$_2$]·2H$_2$O (complex 4).** A methanolic solution (5 mL) containing Hfluf (45 mg, 0.16 mmol) and KOH (9 mg, 0.16 mmol) was stirred for 1 h. The resultant solution was added into the methanolic solution (5 mL) of CuCl$_2$·2H$_2$O (28 mg, 0.16 mmol) simultaneously with a methanolic solution (10 mL) of HL (20 mg, 0.08 mmol). The mixture was stirred for 30 min and then left to cool at room temperature. A brown precipitate was formed and separated by filtration. The filtrate was left for slow evaporation at room temperature and green single-crystals of complex **4** (20 mg, 25%) suitable for X-ray determination were collected after one week. Elemental analysis: calcd for [Cu$_4$(L$^1$)$_2$(fluf)$_4$(Cl)$_2$]·2H$_2$O ($C_{86}H_{64}Cl_2Cu_4F_{12}N_{14}O_{12}$, MW = 2038.61): C 50.67, H 3.16, N 9.62; found: C 50.55, H 3.34, N 9.75%. IR (KBr disk), $\nu$ (cm$^{-1}$): $\nu$(C═N): 1617 (s); $\nu_{asym}$(COO): 1585 (s); $\nu_{sym}$(COO): 1410 (m); $\Delta\nu$(COO) = 175; $\nu$(Cu–N): 525 (m). The complex is insoluble in the solvents tested.

### 2.3 X-ray crystal structure determination

Suitable single-crystals of the complexes were mounted on thin glass fibers with the aid of epoxy resin. X-ray diffraction data were recorded using a Bruker Kappa Apex II CCD area-detector diffractometer, equipped with a Mo Kα ($\lambda$ = 0.71073 Å) sealed tube source and a Triumph monochromator at 295 K, using the $\varphi$ and $\omega$ scans technique. The program Apex2 (Bruker AXS, 2006) was used for data collection and cell refinement. The collected data were integrated with the Bruker SAINT software package[43] using a narrow-frame algorithm. Data were corrected for absorption using the numerical method SADABS,[44] based on the crystal dimensions. Structures were solved using the SUPERFLIP package[45] and refined with full-matrix least-squares on $F^2$ using the Crystals program package version 14.61 build 6236.[46] Anisotropic displacement parameters were applied to all non-hydrogen atoms of the complexes and the non-disordered solvent atoms, while hydrogen atoms were in general found and/or positioned geometrically and refined using a riding model. Details of crystal data and structure refinement parameters are shown in Tables S1 and S2.†

### 2.4 Study of the biological profile of the compounds

All the procedures and relevant equations used in the *in vitro* studies of the biological activity of the compounds (antioxidant activity, interaction with CT DNA, (photo)cleavage of pDNA, and affinity for BSA) can be found in the ESI file (Sections S1–S4†).

## 3 Results and discussion

### 3.1 Synthesis and characterization

The synthesis and characterization of (*E*)-4-(2-(pyridin-2-ylmethylene)hydrazinyl)quinazoline (HL) have been previously reported by our group.[31] The aerobic reaction of quinazoline (HL) with Cu(II) and the corresponding deprotonated NSAIDs led to the formation of complexes **1–4**. Particularly for the synthesis of complex **2**, the quinazoline was reacted previously with complex [Cu(mef)$_2$(H$_2$O)$_2$],[39] since the one-pot reaction,

as applied for the preparation of the other complexes, did not yield any product. The resultant coordination compounds were characterized using IR and UV-vis spectroscopy and single-crystal X-ray crystallography.

In the case of complexes **1** and **4**, the *in situ* formation of the methoxy derivative of HL (Fig. 2), *i.e.* the addition of the methoxy group –OMe on the imino carbon atom, leading to ligand $HL^1$, was observed in their molecular structures as discussed below. In general, such addition of the methoxy group catalyzed by the presence of a metal is described in organic synthesis as C–O bond formation through transition metal-mediated etherification; in the present case, it could be considered a 'copper-mediated methoxylation'[47–49] and may affect the biological behavior of the molecule.[50]

The complexes are stable in air, soluble in DMSO and insoluble in $H_2O$. The molar conductivity values ($\Lambda_M$) of complexes **1–3** were recorded in a 1 mM DMSO solution, and their values were in the range of 2–17 mho $cm^2$ $mol^{-1}$ suggesting that the complexes are not electrolytes.[51] The complexes were characterized using IR and UV-vis spectroscopy and single-crystal X-ray crystallography.

The IR spectra of the complexes are rather complicated since there are many peaks attributed to the characteristic groups of the quinazoline and the NSAID ligands. In brief, the coordination of quinazoline ligands was verified from the presence of a characteristic band in the range 1577–1634 $cm^{-1}$ assigned to $\nu$(C=N) and a medium intensity band in the region 520–526 $cm^{-1}$ which is assigned to $\nu$(Cu–N) and is not observed in the spectrum of free HL.[31–34] On the other hand, the existence and coordination of the NSAID ligands were confirmed from the presence of two strong bands in the regions 1575–1600 $cm^{-1}$ and 1359–1419 $cm^{-1}$ which are attributed to the antisymmetric ($\nu_{asym}$(COO)) and symmetric ($\nu_{sym}$(COO)) stretching vibrations of their carboxylato group, respectively, as well as their difference $\Delta\nu$(COO) (= $\nu_{asym}$(COO) − $\nu_{sym}$(COO)) with values equal to 175–216 $cm^{-1}$ indicating diverse modes of coordination.[52]

The UV-vis spectra of the complexes and ligands were recorded both in DMSO solution and as Nujol mulls. The spectra of all compounds in the solid state (Nujol) displayed similar patterns to those observed in DMSO solution, indicating that the complexes are likely stable in solution. In the visible region of the electronic spectra of complexes **1–3**, one band was observed in the region 645–695 nm ($\varepsilon$ = 30–95 $M^{-1}$ $cm^{-1}$) which is attributed to d–d transition, characteristic of Cu(II) complexes with a square pyramidal geometry.[53] Furthermore, all the complexes exhibit at least three bands which are also present in the spectrum of HL and can be attributed to its intra-ligand (n → π* and π → π*) transitions.[54]

### 3.2 Structure of the complexes

The molecular structures of all complexes **1–4** were determined using single-crystal X-ray crystallography. All crystallographic experimental data are summarized in Tables S1 and S2.†

Complex **1** crystallizes in the monoclinic system and $P2_1/c$ space group (Table S1†). The molecular structure is given in Fig. 3, and selected bond lengths and angles are provided in Tables 1 and S3.†

It is a polymeric Cu(II) complex consisting of a mononuclear repeating unit [Cu($HL^1$)(μ-Cl)](difl) containing the cationic complex [Cu($HL^1$)(μ-Cl)]$^+$ and a $difl^{-1}$ anion as a counterion in the crystal lattice. The chlorido ligands function as bridging ligands between two adjacent Cu(II) ions, thus facilitating the formation of the polymeric structure. The quinazoline ligand $HL^1$ is formed *in situ* in the reaction solution bearing a $CH_3O$-group attached to the C9 atom, is neutral and is coordinated to the Cu1 ion in a tridentate manner through three nitrogen atoms, *i.e.* the quinazoline N1, the hydrazone N4, and the pyridine N5, forming two chelating five-membered rings. Cu(II) ion is penta-coordinated and its coordination sphere $CuN_3Cl_2$ comprises three nitrogen atoms from the $HL^1$ ligand and two bridging chlorido ligands. The trigonality index, defined as $\tau_5 = (\varphi_1 - \varphi_2)/60°$ (where $\varphi_1$ and $\varphi_2$ are the largest angles in the coordination sphere; $\tau_5 = 0$ is found for a perfect square pyramid and $\tau_5 = 1$ for a perfect trigonal bipyramid),[55] is $\tau_5 = (162.99–158.69)/60 = 0.07$ suggesting a slightly distorted square pyramidal geometry around the Cu atom, with N1, N4, N5, and Cl1 (which are almost co-planar) forming the base of the pyramid. The bridging $Cl1^i$ of an adjacent layer is at the apex at an elongated Cu1–$Cl1^i$ distance of 2.7175(7) Å, as expected for μ-chlorido-bridged Cu(II) complexes.[56,57] The $Cu1^{ii}$–Cl1–Cu1 angle has a value of 100.13(2)° showing the non-linearity of the three atoms and is rather close to angle values found for μ-chlorido-bridged Cu(II) complexes (in the range of 107.38–179°).[56–59]

As a result of this bent Cu1–Cl1–Cu1 angle, the interatomic Cu···Cu distance is 3.818 Å and is in the range (3.782–5.106 Å) found for Cu(II) ions bearing one chlorido-bridge.[59–62] The

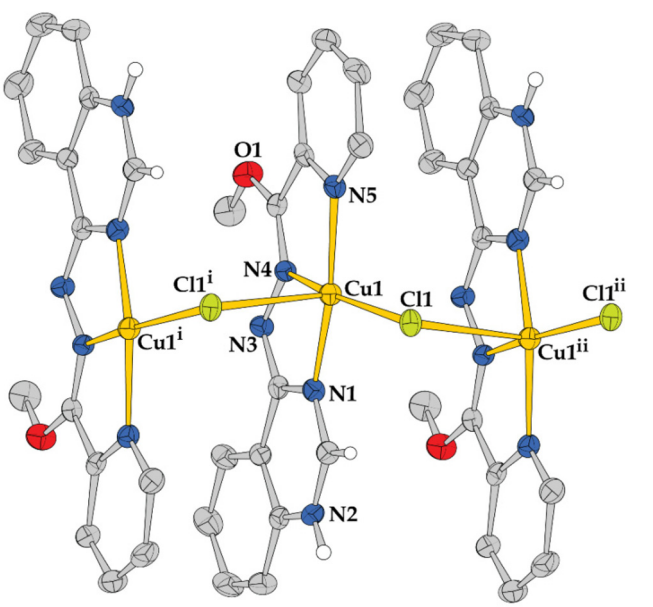


**Fig. 3** The molecular structure of complex **1**. Methyl and most aromatic H atoms as well as the $difl^{-1}$ counterions are omitted for clarity. Symmetry codes: (i) *x*, –*y* + 3/2, *z*–1/2; (ii) *x*, –*y* + 3/2, *z* + 1/2.

**Table 1** Selected bond lengths (Å) and angles (°) for complexes **1–4**

| Bond | Length (Å) | Bond | Length (Å) | Bond | Angle (°) |
|---|---|---|---|---|---|
| Complex **1** | | | | | |
| Cu1–Cl1 | 2.2459(6) | Cu1–N5 | 2.0122(19) | N1–Cu1–N5 | 158.69 (8) |
| Cu1–N1 | 1.977(2) | Cu1–Cl1$^{i}$ | 2.7175(7) | N4–Cu1–Cl1 | 162.99 (6) |
| Cu1–N4 | 1.9559(19) | Cu···Cu$^{i}$ | 3.818 | Cl1$^{i}$–Cu1–Cl1 | 97.72 (2) |
| | | | | Cu1$^{ii}$–Cl1–Cu1 | 100.13 (2) |
| Complex **2** | | | | | |
| Cu1–O2 | 1.944 (2) | Cu1–N4 | 1.942 (2) | N1–Cu1–N5 | 158.30 (10) |
| Cu1–O3 | 2.337 (3) | Cu1–N5 | 2.049 (3) | O2–Cu1–N4 | 175.52 (11) |
| Cu1–N1 | 1.984 (2) | | | | |
| Complex **3** | | | | | |
| Cu1–N5$^{i}$ | 2.056 (4) | Cu1–N4$^{i}$ | 1.962 (4) | N5$^{i}$–Cu1–N1$^{i}$ | 156.65 (16) |
| Cu1–N1$^{i}$ | 1.993 (3) | Cu1–O1 | 1.927 (3) | N4$^{i}$–Cu1–O1 | 162.26 (15) |
| Cu1–N2 | 2.281 (3) | | | | |
| Complex **4** | | | | | |
| Cu1–O1 | 1.963(2) | Cu2–N1 | 1.943 (3) | O1–Cu1–O2 | 167.06 (8) |
| Cu1–O2 | 1.957(2) | Cu2–N4 | 1.971 (3) | O3–Cu1–O4 | 167.18 (7) |
| Cu1–O3 | 1.9728(17) | Cu2–N5 | 2.004 (3) | N4–Cu2–Cl1 | 179.19 (9) |
| Cu1–O4 | 1.9685(17) | Cu2–Cl1 | 2.1897 (10) | N1–Cu2–N5 | 158.54 (11) |
| Cu1–N2 | 2.195(2) | Cu1···Cu1$^{i}$ | 2.6568 (7) | | |

Symmetry codes for complex **1**: (i) $x$, $-y + 3/2$, $z - 1/2$ and (ii) $x$, $-y + 3/2$, $z + 1/2$; for complex **3**: (i) $x + 1/2$, $-y + 1/2$, $-z + 1$; for complex **4**: (i) $-x + 1$, $-y + 1$, $-z + 1$.

Cu···Cu distance reported is in the range 3.4874–4.776 Å for complexes with two chlorido-bridges[63–65] and 3.192 Å for the rare case of a tri-μ-chlorido-bridged complex.[66] The structure of the complex is further stabilized by hydrogen bonds. More specifically, the anion of diflunisal is stabilized in the lattice through hydrogen bonds developed between its carboxylate O3 and the hydrogen H21 of the quinazoline nitrogen N2 (Table S4†).

Complex **2** is a neutral mononuclear Cu(II) complex that crystallizes in the monoclinic system and $P2_1/n$ space group (Table S1†). The molecular structure of the complex is shown in Fig. 4 and selected bond lengths and angles are listed in Tables S5† and 1.

In this complex, the Cu1 ion is five-coordinated with a $CuN_3O_2$ coordination sphere. The quinazoline ligand ($L^-$) is deprotonated (for the first time reported) at N2 of the quinazoline ring and is coordinated to the Cu1 ion in a tridentate bichelating manner through the quinazoline N1, hydrazone N4, and pyridine N5 nitrogen atoms, similarly to its previously reported complexes.[31–34] The coordination sphere is completed with two oxygen atoms: one carboxylato oxygen O2 from the deprotonated monodentate mefenamato ligand and a methanol oxygen O3. According to the trigonality index $\tau_5$ = (172.51–158.30)/60 = 0.29,[55] the geometry around the Cu1 ion can be described as a distorted square pyramid with O2, N1, N4, and N5 forming the basal plane (the Cu1–O/$N_{base}$ distances are in the range 1.942(2)–2.049(3) Å and the sum of the base angles is 359° suggesting the co-planarity of these atoms) and O3 being at the apex of the pyramid with a Cu1–O3 distance of 2.337(3) Å. The non-coordinated carboxylato oxygen O1 of the mefenamato ligand lies at 2.731(3) Å, contributing to a rather pseudo-octahedral geometry.

The structure of the complex is stabilized by hydrogen bonds. More specifically, intraligand H-bonds between the amino H61 and the coordinated carboxylato O2 of the mefenamato ligand are developed. The methanol solvate molecule participates in the formation of two H-bonds with the methanol ligand and quinazoline N2$^{i}$ of an adjacent molecule and is thus stabilized in the lattice (Table S4†).

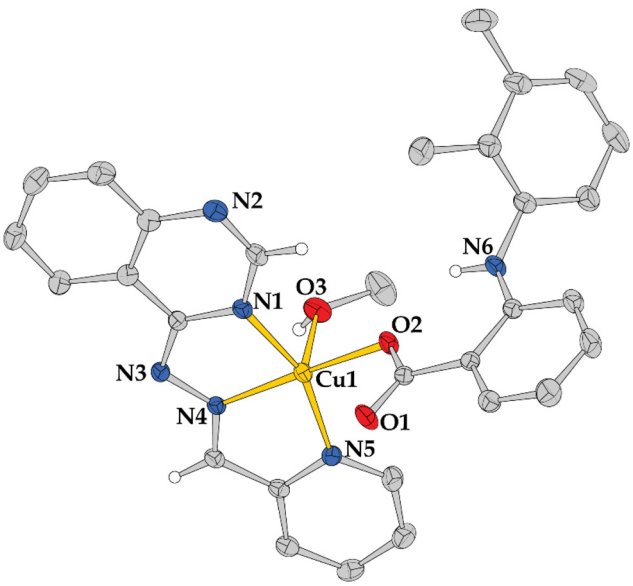


**Fig. 4** The molecular structure of complex **2**. The solvate methanol molecule and aromatic and methyl H atoms are omitted for clarity.

Complex **3** is a polymeric Cu(II) complex crystallized in the orthorhombic system with the $P2_12_12_1$ space group (Table S2†). The molecular structure of the complex is depicted in Fig. 5 and selected bond lengths and angles are listed in Tables S6† and 1.

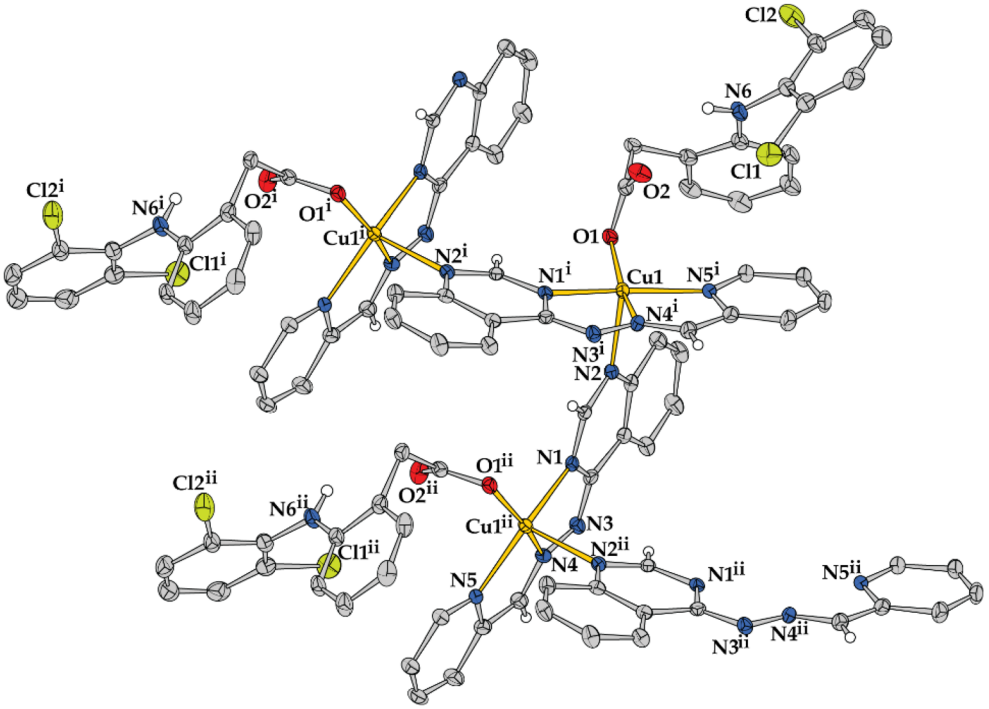


**Fig. 5** The molecular structure of complex **3**. The aromatic H atoms are omitted for clarity. Symmetry codes: (i) $x + 1/2, -y + 1/2, -z + 1$; and (ii) $x - 1/2, -y + 1/2, -z + 1$.

The asymmetric unit of the complex contains a Cu(II) ion, a deprotonated quinazoline ($L^-$) and a deprotonated diclofenac ligand ($dicl^{-1}$). Each Cu1 ion generally is penta-coordinated with a $CuN_4O$ coordination sphere which contains N1, N4 and N5 of one quinazoline ligand, N2 from a second quinazoline ligand and oxygen O1 from the monodentate diclofenac ligand. The quinazoline ligand is deprotonated and is bound in the tetradentate mode; the quinazoline $N1^i$, the hydrazone $N4^i$, and the pyridine $N5^i$ bind to the Cu1 ion forming two five-membered chelate rings and the deprotonated quinazoline nitrogen $N2^i$ is bound to an adjacent $Cu1^i$ ion. According to the trigonality index $\tau_5 = 0.09$ ((162.26-156.65)/60), the geometry around Cu1 is described as a slightly distorted square pyramid[55] with O1, $N1^i$, $N4^i$ and $N5^i$ forming the base of the pyramid and N2 being at the apical position (Cu1–N2 = 2.281 (3) Å). The Cu1–$O/N_{base}$ distances are in the range 1.927(3)–2.056(4) Å and the interatomic Cu1···$Cu1^i$ distance (they are bridged *via* $N1^i$–$C1^i$–$N2^i$) is 6.043 Å. The intra-ligand H-bond developed between the amino H62 and the non-coordinated carboxylato O2 of the diclofenac ligand stabilizes the structure further (Table S4†).

Complex **4** crystallized in a triclinic system and the $P\bar{1}$ space group (Table S2†). The molecular structure of the complex is shown in Fig. 6 and selected bond lengths and angles are listed in Tables S7† and 1.

It is a neutral tetranuclear Cu(II) complex containing four Cu(II) ions, four flufenamato ligands, two deprotonated $(L^1)^-$ ligands and two chlorido ligands. The structure of the complex is centrosymmetric and can be described as 'two $[Cu(L^1)Cl]$ complexes bridged *via* a dinuclear $[Cu_2(flufenamato)_4]$ complex'. The structure of the dinuclear complex bears the typical paddlewheel motif reported for many copper(II) carboxylato complexes with the molecular formula $[Cu_2(\mu\text{-carboxylato-O,O}')_4(L)_2]$, where L = O- or N-donor.[35,40,67,68] In particular, the four deprotonated bidentate flufenamato ligands form *syn–syn* carboxylato bridges between the two isolated copper ions, Cu1 and $Cu1^i$, which are separated by 2.6568(7) Å. The Cu1 and $Cu1^i$ ions are penta-coordinated with $CuNO_4$ coordination spheres which include four carboxylato oxygen atoms (one from each flufenamato ligand) and a nitrogen atom (N2) from the adjacent 'mononuclear' $[Cu(L^1)Cl]$ complex. Based on the value of the trigonality index $\tau_5 = 0.002$ ((167.18–157.06)/60), the geometry around the Cu1 and $Cu1^i$ ions is square pyramidal,[55] with the four oxygen atoms forming the basal plane and N2 being at the apical position (Cu1–N2 = 2.195(2) Å).

In the two $[Cu(L^1)Cl]$ complexes, the deprotonated quinazoline ligands $(L^1)^-$ are bound in the tetradentate mode similar to that of the L ligand in complex **3**; they are coordinated to Cu2 and $Cu2^i$ ions *via* the quinazoline, the hydrazone and the pyridine nitrogen atoms (N1, N4, and N5, respectively) in a tridentate bichelating fashion while the deprotonated quinazoline nitrogen atoms N2 lie at the apical positions of Cu1 and $Cu1^i$ ions as previously mentioned. The interatomic Cu1···Cu2 distance (bridged *via* N1–C1–N2) is 5.854 Å. The Cu2 and $Cu2^i$ ions are tetra-coordinated with a $CuN_3Cl$ coordination sphere and square planar geometry (as concluded from (i) the sum of the angles around Cu2 which is 359.99°, (ii) the tetrahedrality value of 5.14° (the tetrahedrality is determined from the angle

 

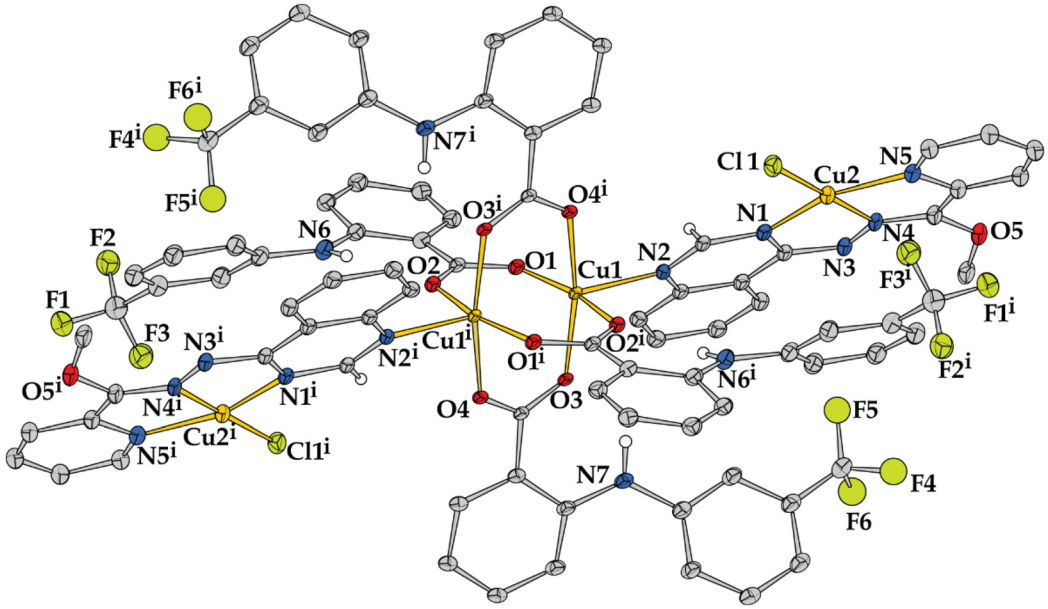


**Fig. 6** The molecular structure of complex **4**. The aromatic H atoms and solvate molecules are omitted for clarity (symmetry code: (i) $-x + 1, -y + 1, -z + 1$).

formed by the two planes enclosing the metal ion (Cu2) and two adjacent coordinated atoms; for square planar complexes ($D_{4h}$ symmetry), tetrahedrality is 0°; for tetrahedral complexes ($D_{2d}$ symmetry), tetrahedrality is 90°),[69] and (iii) the tetrahedral index $\tau_4 = 0.16$, as introduced by Yang ($\tau_4 = (360° - (\alpha + \beta))/(360° - 2 \times 109.5°)$, where $\alpha$ and $\beta$ are the largest angles around the metal),[70] or $\tau'_4 = 0.10$, as introduced by Okuniewski ($\tau'_4 = ((\beta - \alpha)/(360° - 109.5°)) + ((180° - \beta)/(180° - 109.5°))$ where $\beta > \alpha$ are the largest angles of the coordination sphere)).[71]

The structure of complex **4** is further stabilized by the development of hydrogen bonds, *i.e.* intraligand H-bonds between the coordinated carboxylato O2 and O3 atoms and the amino H61 and H71 atoms, respectively, of the flufenamato ligands, and intermolecular H-bonds between the hydrogen atoms of the solvate water molecules and coordinated oxygen atoms of the flufenamato ligands (Table S4†).

A brief comparison of the bond distances between Cu(II) ions and nitrogen atoms of quinazoline ligands in complexes **1–4** with the corresponding bond distances previously reported for diverse metal complexes of HL and its halogenated derivatives (*E*)-4-(2-((3-fluoropyridin-2-yl)methylene)hydrazinyl) quinazoline ($HL^2$) and (*E*)-4-(2-((6-bromopyridin-2-yl)methylene) hydrazinyl)quinazoline ($HL^3$) reveals that, with the exception of Co(III)–N bond distances found in the complex $[Co(HL)_2](NO_3)_3$,[32] the Cu(II)–N bond distances found in complexes **1–4** are among the shortest ones observed for metal(II)–$N_{(HL)}$ in these complexes (Table 2). In almost all of these complexes, the metal–$N_{hydrazone}$ bond distances are the shortest metal–N bond distances in the coordination sphere and the metal–$N_{pyridine}$ distances are the longest ones (Table 2).[31–34] Specifically for the reported copper(II) complexes, the neutral complexes **1–4** and $[Cu(HL^2)(Cl)_2]$[34] presented shorter Cu(II)–N

**Table 2** Comparison of selected bond distances (Å) for complexes **1–4** and previously reported metal-quinazoline analogues

| Compound | M–$N_q$[a] (Å) | M–$N_h$[a] (Å) | M–$N_p$[a] (Å) | Ref. |
|---|---|---|---|---|
| Complex **1** | 1.977(2) | 1.9559(19) | 2.0122(19) | tw[b] |
| Complex **2** | 1.984(2) | 1.942(2) | 2.049(3) | tw[b] |
| Complex **3** | 1.993(3) | 1.962(4) | 2.056(4) | tw[b] |
| Complex **4** | 1.943(3) | 1.971(3) | 2.004(3) | tw[b] |
| $[Cu(HL)_2]Cl_2$ | 2.110(3) | 2.001(2) | 2.132(3) | 32 |
| $[Ni(HL)_2]Cl_2$ | 2.105(3) | 1.993(2) | 2.126(2) | 32 |
| $[Ni(HL)_2](NO_3)_2$ | 2.077(3), 2.098(3) | 2.000(3), 2.011(3) | 2.130(3), 2.132(3) | 32 |
| $[Zn(HL)_2](NO_3)_2$ | 2.188(2) | 2.070(2) | 2.199(2) | 31 |
| $[Zn(HL)(dicl)_2]$ | 2.169(4) | 2.133(3) | 2.238(4) | 31 |
| $[Mn(HL)(Cl)_2]$ | 2.268(3) | 2.198(3) | 2.269(3) | 33 |
| $[Mn(HL)(H_2O)(HCOO)Cl]$ | 2.301(2) | 2.258(2) | 2.319(3) | 33 |
| $[Co(HL)_2]Cl_2$ | 2.105(2) | 1.9964(18) | 2.132(2) | 32 |
| $[Co(HL)_2](NO_3)_2$ | 2.206(2) | 2.085(2) | 2.186(3) | 32 |
| $[Co(HL)_2](NO_3)_3$ | 1.912(2), 1.931(2) | 1.836(3), 1.871(2) | 1.934(3), 1.950(2) | 32 |
| $[Cd(HL)(Cl)_2]$ | 2.375(3) | 2.308(3) | 2.366(3) | 32 |
| $[Cd(HL)(CH_3OH)(H_2O)(NO_3)](NO_3)$ | 2.365(3) | 2.318(3) | 2.380(3) | 32 |
| $[Cu(HL^2)(Cl)_2]$[c] | 1.986(4) | 1.959(4) | 2.043(4) | 34 |
| $[Zn(HL^2)_2](NO_3)(PF_6)$ | 2.139(2), 2.135(2) | 2.070(2), 2.090(2) | 2.271(2), 2.253(2) | 34 |
| $[Cd(HL^2)(H_2O)(CH_3OH)(NO_3)](NO_3)$ | 2.348(3) | 2.339(3) | 2.377(3) | 34 |
| $[Ni(HL^2)_2](NO_3)_2$ | 2.105(3), 2.097(2) | 1.984(3), 1.988(2) | 2.129(3), 2.141(3) | 34 |
| $[Mn(HL^2)(CH_3OH)(Cl)_2]$ | 2.254(3) | 2.234(2) | 2.299(3) | 34 |
| $[Ni(HL^3)_2](NO_3)_2$[d] | 2.088(3) | 2.007(3) | 2.189(3) | 34 |

[a] $N_q$ = quinazoline N; $N_h$ = hydrazone N; $N_p$ = pyridine N. [b] tw = this work. [c] $HL^2$ = (*E*)-4-(2-((3-Fluoropyridin-2-yl)methylene)hydrazinyl)quinazoline. [d] $HL^3$ = (*E*)-4-(2-((6-Bromopyridin-2-yl)methylene)hydrazinyl) quinazoline.

bond distances (Cu(II)–$N_{hydrazone}$ = 1.942(2)–1.971(3) Å, Cu(II)–$N_{quinazoline}$ = 1.943(3)–1.993(3) Å, and Cu(II)–$N_{pyridine}$ = 2.004(3)–2.056(4) Å) than those reported for the cationic complex $[Cu(HL)_2]Cl_2$ (Cu(II)–$N_{hydrazone}$ = 2.001(2) Å, Cu(II)–$N_{quinazoline}$ = 2.110(3) Å and Cu(II)–$N_{pyridine}$ = 2.132(3) Å).[32]

### 3.3 Interaction of the complexes with CT DNA

The interaction of the compounds with CT DNA was studied directly by UV-vis spectroscopic titrations and DNA-viscosity measurements and indirectly through competitive studies with EB with fluorescence emission spectroscopy.

UV-vis spectroscopy is a fundamental technique for the initial assessment of how the compounds interact with DNA. It can offer valuable insights into the interaction mode (whether covalent or noncovalent interactions, or even cleavage, occur) and help calculate its strength through the DNA-binding constant ($K_b$). During UV-vis spectroscopic titrations, any changes in the charge-transfer or intraligand bands of the compounds can be monitored. These experiments may provide the first indication of DNA interaction, as shifts or alterations in the bands of the compounds could suggest the presence of intercalation or other binding mechanisms.

The UV-vis spectra of the compounds were recorded in the presence of increasing concentrations of CT DNA solutions (Fig. S1†). The alterations observed in the bands of the complexes were rather complicated including hypochromism and/or hyperchromism, accompanied by hypsochromic and/or bathochromic shifts (Table 3). Such changes in the UV-vis spectra may confirm the interaction between the compounds and CT DNA suggesting the formation of a new DNA–complex adduct. The overall changes in the electronic spectra suggest an interaction between the complexes and CT DNA; however, a clear interaction mode cannot be determined necessitating more experiments such as DNA-viscosity measurements and competitive studies with EB.

The DNA-binding constants of the compounds (Table 3) were calculated using the Wolfe–Shimer equation (eqn (S1)†)[72] and the corresponding plots of [DNA]/($\varepsilon_A - \varepsilon_f$) *versus* [DNA] (Fig. S2†). Complexes **1–3** interact tightly with CT DNA and present higher $K_b$ than the classic intercalator EB (= $1.23 \times 10^5$ $M^{-1}$).[73] The DNA-binding constants of complexes **1–3** studied herein fall in the same range as the $K_b$ values reported for diverse metal complexes bearing HL or its halogenated derivatives as ligands.[31–34]

The measurements of the viscosity of a CT DNA solution were conducted to determine the type of interaction between the complexes and DNA. DNA viscosity is sensitive to changes in length (relative DNA viscosity is proportional to the relative DNA length), making it a useful technique to investigate the interaction mode between compounds and DNA. A significant increase in DNA viscosity typically results from classic intercalative agents, which penetrate DNA bases and thus increase the overall DNA length. Less pronounced or no changes in DNA viscosity usually indicate nonclassical intercalation (*i.e.* external interaction including groove-binding or electrostatic interactions).[74,75] The viscosity of a CT DNA solution (0.1 mM) was monitored with the addition of increasing amounts of complexes **1–3** (up to a ratio value of $r$ = 0.36, Fig. 7). Initially (for $r$ values up to 0.10), a slight lowering of relative DNA viscosity was observed suggesting an initial external interaction letting the compounds approach closer to DNA. Afterwards, the relative DNA viscosity increased significantly, suggesting that the complexes may intercalate to CT DNA.

As a typical DNA intercalation marker, EB intercalates between adjacent DNA base pairs. When a solution containing the EB–DNA complex is subjected to excitation at 540 nm, an intense emission band characteristic of EB–DNA appears at

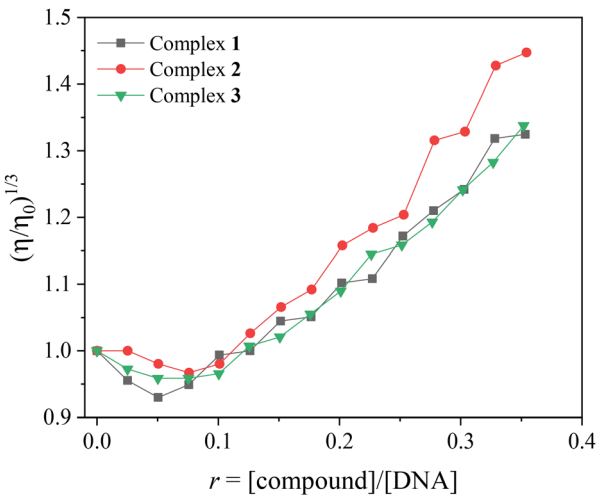


**Fig. 7** Relative viscosity of CT DNA $(\eta/\eta_0)^{1/3}$ in buffer solution (150 mM NaCl and 15 mM trisodium citrate, pH 7.0) in the presence of complexes **1–3** at increasing amounts ($r$ = [compound]/[DNA]).

**Table 3** UV-vis spectral features of the interaction of complexes **1–3** with CT DNA. UV-vis bands ($\lambda_{max}$, in nm), percentage of observed hyper-/hypo-chromism ($\Delta A/A_0$, in %), blue-/red-shift of $\lambda_{max}$ ($\Delta\lambda$, nm), and DNA-binding constants ($K_b$, in $M^{-1}$)

| Compound | Band $\lambda_{max}$ (nm) ($\Delta A/A_0$[a] (%), $\Delta\lambda$[b] (nm)) | $K_b$ ($M^{-1}$) |
|---|---|---|
| Complex **1** | 287(sh)[c] (−17, elim[d]); 309(sh) (−21, elim); 372(sh) (−51, elim); 395(sh) (−29, elim); 424 (+12, +3); 457(sh) (+23, −6) | $1.80(\pm 0.01) \times 10^7$ |
| Complex **2** | 294 (+8, +5); 339 (sh) (−13, elim); 440 (sh) (+4, −3); 466 (−13, −5) | $6.69(\pm 0.11) \times 10^5$ |
| Complex **3** | 279(+4, +5); 439(sh) (−2, −1); 464 (−12, −6) | $4.62(\pm 0.04) \times 10^5$ |
| HL [31] | 294(−3, −2); 365(−8, 0); 433(sh) (+5, 0) | $5.70(\pm 0.27) \times 10^5$ |

[a] "+" denotes hyperchromism and "–" denotes hypochromism. [b] "+" denotes red-shift and "–" denotes blue-shift. [c] "sh" = shoulder. [d] "elim" = eliminated.

592–594 nm. The competition of the complexes with EB for DNA intercalation sites may confirm the intercalation of the compounds into DNA.[76] The EB–DNA conjugate was formed after 1 h of pre-treatment of an EB solution (20 μM) with CT DNA (26 μM) and exhibited an intense fluorescence emission band at 593 nm. The fluorescence emission spectra ($\lambda_{exc}$ = 540 nm) of the EB–DNA solution were recorded with increasing concentrations of the compounds (shown representatively for complex **2** in Fig. 8(A)) and the characteristic emission band showed a significant quenching (up to 84.2% of the initial EB–DNA fluorescence, Fig. 8(B) and Table 4), verifying the displacement of EB from EB–DNA.

The observed quenching agrees with the linear Stern–Volmer equation (eqn (S2) and (S3)†) according to the corresponding Stern–Volmer plots ($R \sim 0.99$, Fig. S3†) where the Stern–Volmer constants ($K_{SV}$) were determined (Table 4). The quenching constants ($K_q$) of complexes **1–3** (Table 4) were calculated using eqn (S3)† applying the value of 23 ns as the fluorescence lifetime of the EB–DNA system ($\tau_0$),[77] and they are significantly higher than the threshold of $10^{10}$ $M^{-1}$ $s^{-1}$, suggesting that the observed quenching occurs through a static quenching mechanism.[76] The high quenching values in combination with the high $K_b$ values lead to the conclusion that the EB molecule can be replaced by the complexes from its EB–DNA adduct because of their intercalation to CT DNA.

**Table 4** Fluorescence features of the EB displacement studies of complexes **1–3**. Percentage of EB–DNA fluorescence emission quenching ($\Delta I/I_0$, in %), Stern–Volmer constants ($K_{SV}$, in $M^{-1}$) and quenching constants ($K_q$, in $M^{-1}$ $s^{-1}$)

| Compound | $\Delta I/I_0$ (%) | $K_{SV}$ ($M^{-1}$) | $K_q$ ($M^{-1}$ $s^{-1}$) |
|---|---|---|---|
| Complex **1** | 71.4 | $6.93(\pm 0.30) \times 10^4$ | $3.01(\pm 0.13) \times 10^{12}$ |
| Complex **2** | 84.2 | $3.05(\pm 0.16) \times 10^5$ | $1.33(\pm 0.07) \times 10^{13}$ |
| Complex **3** | 67.9 | $3.47(\pm 0.16) \times 10^5$ | $1.51(\pm 0.05) \times 10^{13}$ |
| HL[31] | 54.4 | $1.05(\pm 0.03) \times 10^5$ | $1.05(\pm 0.03) \times 10^{13}$ |

### 3.4 Interaction of the compounds with plasmid DNA

The ability of the compounds to interact with DNA, combined with their diverse electronic spectra, prompted investigations into the degradation of plasmid DNA both in the presence and absence of irradiation. This research aimed to assess the compounds' potential as synthetic nucleic acid degradation agents and their capacity for photoactivation. Initially, the compounds were dissolved in DMSO at various concentrations (500 μM, 300 μM, 200 μM, and 100 μM) and combined with a Tris buffer solution (25 μM, pH 6.8) that contained pDNA (Form I). The DMSO concentration in the final solution was maintained below 10% v/v. The effectiveness of the complexes in degrading pDNA was evaluated through gel electrophoresis. The free NSAIDs diflunisal, mefenamic acid and diclofenac did not show any significant ability to cleave pDNA during the experiments. During electrophoresis, the supercoiled pDNA appears as Form I in the gel. The extent of DNA damage was assessed by calculating the percentage of single-stranded (ss) and double-stranded (ds) DNA affected. The DNA was categorized into three forms: Form I (supercoiled), Form II (relaxed), and Form III (linear plasmid DNA). The ss% and ds% damage were calculated according to eqn (S4) and (S5).†

The reaction mixtures were incubated in the dark for 150 min and then analyzed by 1% agarose gel electrophoresis with EB staining. In the absence of light, compounds **1** and **2** (500 μM) did not practically cleave pDNA (Fig. 9, Lanes 2 and 3). Quite similar was the behavior of HL and its copper(II)

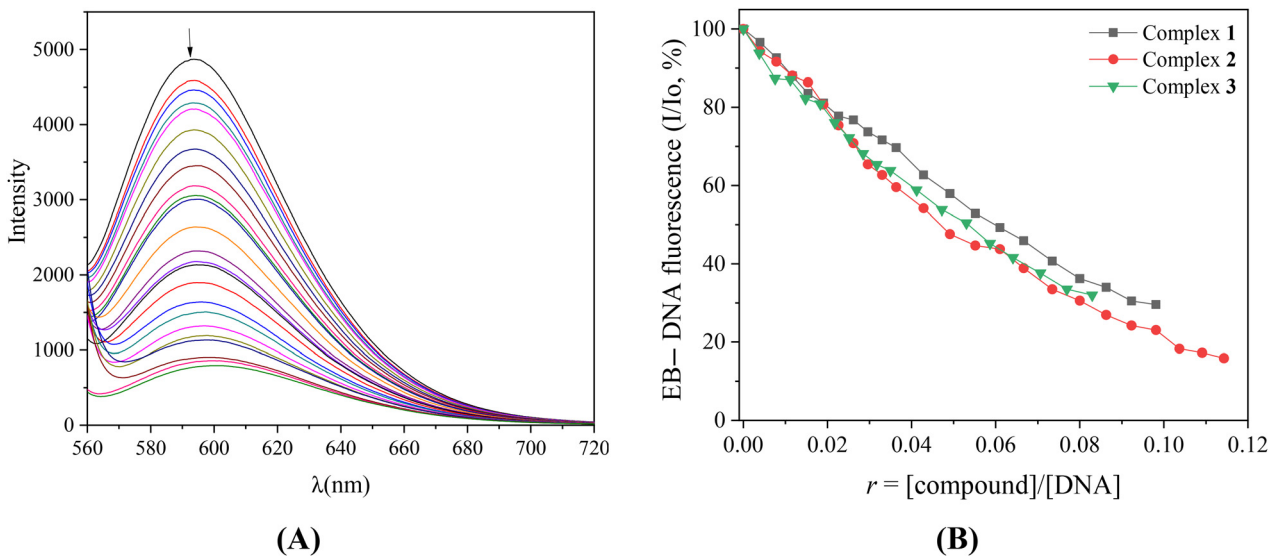


**Fig. 8** (A) Fluorescence emission spectra ($\lambda_{excitation}$ = 540 nm) of EB–DNA ([EB] = 20 μM, [DNA] = 26 μM) in buffer solution in the absence and presence of increasing amounts of complex **2** ($r$ = [compound]/[DNA] = 0–0.12). The arrow shows the changes in intensity upon increasing the amounts of the complex. (B) Plot of relative EB–DNA fluorescence intensity ($I/I_0$, %) at $\lambda_{emission}$ = 592 nm *versus* $r$ ($r$ = [compound]/[DNA]) in the presence of complexes **1–3** (up to 28.6% of the initial EB–DNA fluorescence for complex **1**, 15.8% for complex **2** and 32.1% for complex **3**).

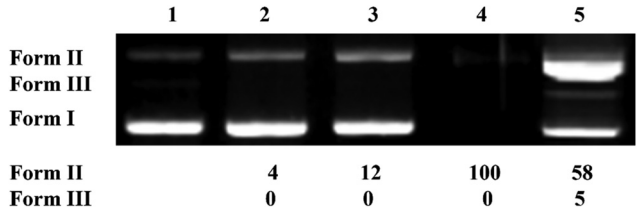


Fig. 9 Agarose gel analysis of pDNA after incubation with complexes **1–3**, stained with EB and run for 60 min of electrophoresis. Top: gel image showing the lanes as follows: Lane 1: pDNA (control), Lane 2: pDNA + complex **1** (500 μM), Lane 3: pDNA + complex **2** (500 μM), Lane 4: pDNA + complex **3** (300 μM), Lane 5: pDNA + complex **3** (200 μM). Bottom: calculation of % damage in single-stranded (ss) and double-stranded (ds) pDNA forms. pDNA forms: Form I = supercoiled, Form II = relaxed, and Form III = linear plasmid DNA.

complex $[Cu(HL)_2]Cl_2$ which were practically inactive under similar conditions.[31,32] In contrast, at high concentrations (300 μM), complex **3** cleaved pDNA into multiple fragments, making them undetectable by EB staining (Fig. 9, Lane 4). At lower concentrations (200 μM), complex **3** induced ss nicks at a percentage of 58% (Fig. 9, Lane 5).

The exposure of pDNA complexes to radiation resulted in more active compounds. Although HL and $[Cu(HL)_2]Cl_2$ were practically inactive after exposure to UVB radiation,[31,32] complex **1** (500 μM) exhibited moderate activity, resulting in approximately 50% ss nicks (Fig. 10(A), Lane 2), while complex **2** (500 μM) showed enhanced but still limited activity (Fig. 10 (A), Lane 3). Complex **3** demonstrated the highest activity among the compounds leading to complete degradation (for concentration ≥300 μM), rendering the DNA undetectable by EB staining (Fig. 10(A), Lane 4). At lower concentrations (200 μM), complex **3** induced 79% ss nicks and 4% ds nicks (Fig. 10(A), Lane 5). Except for complex **1** which presented significantly higher activity, UVB irradiation did not seem to affect the activity of the compounds, as they were capable of cleaving DNA even without light exposure.

After exposure of the pDNA complex to UVA radiation, the activity of complexes **1** and **2** increased (Fig. 10(B), Lanes 2 and 3), inducing damage to pDNA at 52% and 35%, respectively. Complex **3** maintained its high activity, although it induced lower damage to pDNA (total damage of 69% at the concentration of 300 μM, Fig. 10(B), Lanes 4 and 5) than in the presence of UVB radiation.

The activity of complexes **2** and **3** decreased (Fig. 10(C), Lanes 3–5) after exposure to visible light, while complex **1** (500 μM) demonstrated its high activity, inducing ss nicks at a percentage of 73% (Fig. 10(C), Lane 2). Complex **3** still is the most active among the compounds since it induced 74% ss nicks at a lower concentration (300 μM, Fig. 10(C), Lane 4).

Complexes **1–3** are more active than HL and $[Cu(HL)_2]Cl_2$ after exposure to any type of radiation used.[31,32] In general, the introduction of the NSAID ligands appears to increase the ability to cleave pDNA in comparison with the free quinazoline HL and the corresponding NSAID-free Cu(II) complex $[Cu(HL)_2]Cl_2$. The irradiation seems to lead to more active compounds whose photocleavage efficacy is dependent on the light used, since complexes **1**, **2** and **3** showed their highest activity after exposure to visible light, UVA and UVB radiation, respectively. Complex **3** is the most active among the compounds tested since its high activity was observed for lower concentrations than the other complexes. The overall (photo) cleavage behavior of the complexes indicates their potential chemotherapeutic effects.

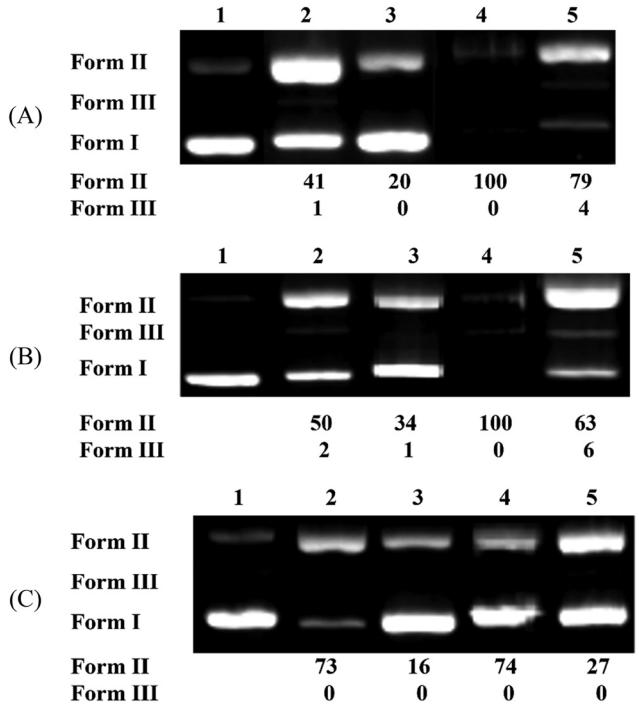


Fig. 10 Agarose gel analysis of pDNA after incubation with complexes **1–3**, exposure to (A) UVB radiation, (B) UVA radiation, (C) visible radiation, and EB staining, followed by 60 min of electrophoresis. Top: gel image showing the lanes as follows: Lane 1: pDNA (control) + radiation; Lane 2: pDNA + complex **1** (500 μM) + radiation; Lane 3: pDNA + complex **2** (500 μM) + radiation; Lane 4: pDNA + complex **3** (300 μM) + radiation; Lane 5: pDNA + complex **3** (200 μM) + radiation. Bottom: calculation of % damage in single-stranded (ss) and double-stranded (ds) pDNA forms. pDNA forms: Form I = supercoiled, Form II = relaxed, and Form III = linear plasmid DNA.

### 3.5 Antioxidant activity of the compounds

The antioxidant activity of complexes **1–3** was evaluated using DPPH and ABTS radical scavenging assays, along with $H_2O_2$ reduction experiments considering that quinazoline derivatives have shown anti-inflammatory activity,[78,79] and their antioxidant profiles may reveal possible effective pharmaceutical applications.[80] Their antioxidant activity was also compared to those of well-established reference antioxidants namely NDGA, BHT, Trolox, and L-ascorbic acid.[80–82]

The scavenging of DPPH radicals is often related to potential anticancer, antiaging process and/or anti-inflammatory activity.[80] Studies on DPPH radical scavenging revealed that complexes **1–3** exhibit low DPPH-scavenging capacity (Table 5), even lower than that of free HL and corresponding NSAIDs Na

Table 5 %DPPH-scavenging ability (DPPH%), %ABTS radical scavenging activity (ABTS%) and $H_2O_2$-reducing ability ($H_2O_2$%) for the compounds. All measurements were carried out in triplicate

| Compound | DPPH%, 20 min/60 min | ABTS% | $H_2O_2$% |
|---|---|---|---|
| Complex **1** | 7.76 ± 0.72/8.09 ± 0.93 | 39.89 ± 0.93 | 66.35 ± 0.72 |
| Complex **2** | 6.37 ± 0.46/5.98 ± 0.36 | 74.69 ± 0.07 | 74.97 ± 0.14 |
| Complex **3** | 9.54 ± 0.42/10.36 ± 0.19 | 71.63 ± 0.94 | 90.11 ± 0.30 |
| HL[31] | 20.63 ± 0.33/21.97 ± 0.69 | 58.91 ± 0.85 | 66.85 ± 0.13 |
| $[Cu(HL)_2]Cl_2$[32] | Negligible/3.33 ± 0.22 | 58.09 ± 1.60 | 70.27 ± 0.22 |
| Hdifl[83] | 10.42 ± 0.56/14.31 ± 0.45 | 76.58 ± 0.74 | 78.46 ± 0.08 |
| Hmef[83] | 5.72 ± 0.08/11.74 ± 0.20 | 66.32 ± 0.38 | 76.42 ± 0.21 |
| Na dicl[83] | 18.26 ± 0.60/17.43 ± 0.23 | 76.35 ± 0.75 | 76.78 ± 0.17 |
| BHT | 61.30 ± 1.16/76.78 ± 1.12 | Not tested | Not tested |
| NDGA | 87.08 ± 0.12/87.47 ± 0.12 | Not tested | Not tested |
| Trolox | Not tested | 98.10 ± 0.48 | Not tested |
| L-Ascorbic acid | Not tested | Not tested | 60.80 ± 0.20 |

dicl, Hmef, and Hdifl, but slightly higher than that of $[Cu(HL)_2]Cl_2$.[32]

Considering the scavenging of the cationic ABTS radicals (such scavenging is indicator of total antioxidant activity), complexes **2** and **3** are the most active among the compounds (74.69 ± 0.07% and 71.63 ± 0.94%, respectively), presenting better activity than HL and $[Cu(HL)_2]Cl_2$[31,32] and similar activity with the free corresponding NSAIDs. Their activity is relatively high, albeit lower than that of the reference compound Trolox (Table 5).

Any compound able to scavenge or reduce $H_2O_2$ is considered a potential agent that can offer relief from oxidative stress and/or inhibit the production of reactive oxygen species.[84] All three complexes present satisfactory activity against hydrogen peroxide and are more active than the reference compound L-ascorbic acid (Table 5). Among the compounds under study, complex **3** stands out, demonstrating the highest $H_2O_2$-reduction capacity at a percentage of 90.11 ± 0.30%.

The overall activity of the complexes is poor against DPPH radicals, moderate-to-significant against ABTS radicals and significant-to-high towards $H_2O_2$. Similar profiles of antioxidant activity were reported for a series of complexes containing HL or its halogenated derivatives.[31–34]

### 3.6 Interaction of the compounds with BSA

The interaction of the complexes with BSA was examined to assess their potential to bind to the most abundant serum protein, albumin,[85] enabling their transport to potential biological targets. This interaction with the most studied albumin, BSA, which is a homologue of human serum albumin, was performed by fluorescence emission quenching experiments.[76] The fluorescence emission spectra of a BSA solution (3 mM) were recorded for $\lambda_{excitation}$ = 295 nm. Incremental addition of the compounds to the BSA solution (Fig. 11(A)) resulted in significant quenching of the fluorescence emission BSA band at 343 nm (the quenching was up to 83.0% of the initial fluorescence intensity, Fig. 11(B) and Table 6). Such quenching is attributed to changes in the secondary structure of the albumin resulting from the association of the compounds with BSA.[76] Furthermore, the inner-filter effect was assessed using eqn (S6)†[86] and it is too low to affect the measurements.

The BSA-quenching constants ($K_q$) associated with the interaction of the compounds with BSA were determined (Table 6) with the Stern–Volmer quenching equation (eqn (S2) and (S3)†) and the corresponding Stern–Volmer plots (Fig. S4†), using the value $\tau_0 = 10^{-8}$ s as the fluorescence lifetime of tryptophan in BSA.[87] The $K_q$ values are of the $10^{13}$ $M^{-1}$ $s^{-1}$ order, exceed significantly the value of $10^{10}$ $M^{-1}$ $s^{-1}$, and indicate the presence of a static fluorescence quenching mechanism,[76] thus confirming the interaction of the compounds with BSA. The $K_q$ values of complexes **1–3** are higher than that of HL and $[Cu(HL)_2]Cl_2$[31,32] with complex **2** exhibiting the highest $K_q$ (= 2.55(±0.09) × $10^{13}$ $M^{-1}$ $s^{-1}$).

The BSA-binding constants ($K$) of complexes **1–3** were calculated with the Scatchard equation (eqn (S7)†) and the corresponding plots (Fig. S5†). For all compounds (Table 6), the binding constants to BSA are of the $10^5$ $M^{-1}$ order, of the same magnitude as that of HL or its halogenated derivatives and their metal complexes,[31–34] and complex **3** presents the highest $K$ (= 5.61(± 0.18) × $10^5$ $M^{-1}$). When comparing the binding constants of the compounds to that of avidin ($K = 10^{15}$ $M^{-1}$), which represents the upper limit for the strongest known non-covalent interactions,[88] it is concluded that the compounds bind reversibly to BSA.

The BSA sites where compounds **1–3** may bind selectively were investigated using competitive binding assays with the most common site-markers warfarin and ibuprofen. Warfarin is a typical site-marker for Sudlow's site 1 (or drug site I) in BSA-subdomain IIA and ibuprofen is a characteristic binder at Sudlow's site 2 (or drug site II) in BSA-subdomain IIIA.[89] Within this context, the fluorescence spectra of BSA were analyzed in the presence of warfarin or ibuprofen upon addition of compounds **1–3** (Fig. 12, S6 and S7†) and the BSA-binding constants in the presence of warfarin or ibuprofen (Table 6) were determined with the Scatchard equation (eqn (S7)†) and corresponding plots (Fig. S8 and S9†).

Any lowering of the BSA-binding constant in the presence of the site-marker may reveal a competitive binding of the compound which is influenced by the presence of the marker inhibiting the approach of the compound towards the same

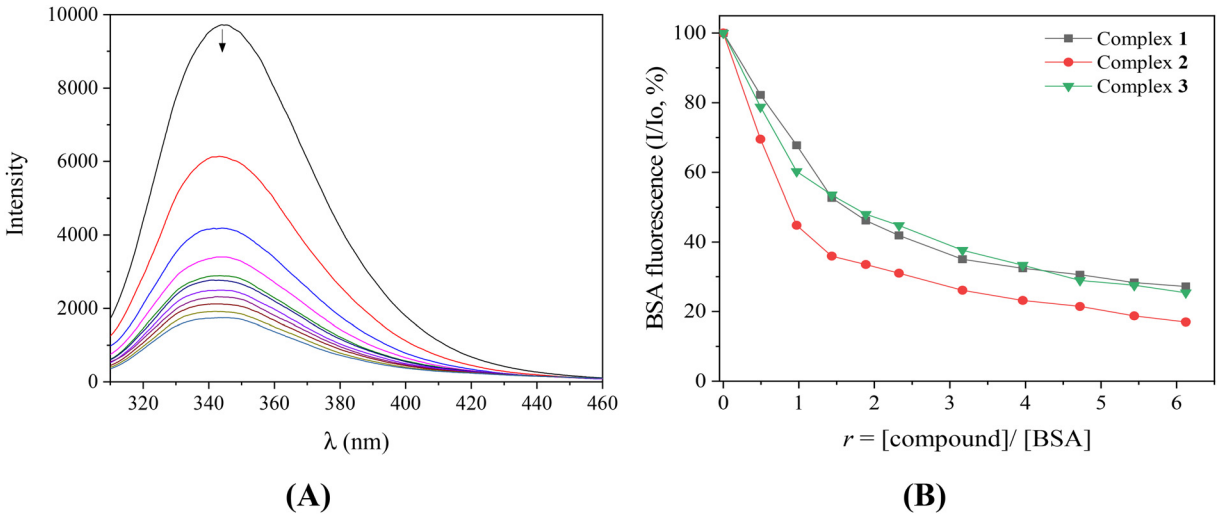


**Fig. 11** (A) Fluorescence emission spectrum ($\lambda_{ex}$ = 295 nm) of a buffer solution (150 mM NaCl, 15 mM sodium citrate, pH 7.0) of BSA (3 μM) in the presence of increasing amounts of complex **2**. The arrow shows the changes in intensity as the concentration of the complex increases. (B) Plot of % relative fluorescence intensity at $\lambda_{em}$ = 343 nm ($I/I_0$, %) *versus r* (*r* = [compound]/[BSA]) for complexes **1–3** (up to 27.2% of the initial BSA fluorescence for **1**, 17.0% for **2**, and 25.4% for **3**).

**Table 6** Fluorescence features of the BSA-binding studies of HL[1] and complexes **1–3**. BSA-quenching constants ($K_q$, in $M^{-1}$ $s^{-1}$) and BSA-binding constants ($K$, in $M^{-1}$) of the compounds in the absence ($K_{(BSA)}$) or presence of a site-marker warfarin ($K_{(BSA,warf)}$) or ibuprofen ($K_{(BSA,ibu)}$)

| Compound | $K_q$ ($M^{-1}$ $s^{-1}$) | $K_{(BSA)}$ ($M^{-1}$) | $K_{(BSA,ibu)}$ ($M^{-1}$) | $K_{(BSA,warf)}$ ($M^{-1}$) |
|---|---|---|---|---|
| Complex **1** | $1.49(\pm 0.08) \times 10^{13}$ | $2.77(\pm 0.11) \times 10^{5}$ | $2.31(\pm 0.12) \times 10^{5}$ | $3.10(\pm 0.13) \times 10^{5}$ |
| Complex **2** | $2.55(\pm 0.09) \times 10^{13}$ | $3.11(\pm 0.15) \times 10^{5}$ | $8.99(\pm 0.19) \times 10^{4}$ | $4.84(\pm 0.12) \times 10^{5}$ |
| Complex **3** | $1.58(\pm 0.04) \times 10^{13}$ | $5.61(\pm 0.18) \times 10^{5}$ | $1.03(\pm 0.04) \times 10^{5}$ | $2.47(\pm 0.11) \times 10^{5}$ |
| HL[31] | $1.05(\pm 0.03) \times 10^{13}$ | $8.68(\pm 0.06) \times 10^{4}$ | $5.18(\pm 0.30) \times 10^{4}$ | $1.03(\pm 0.07) \times 10^{5}$ |

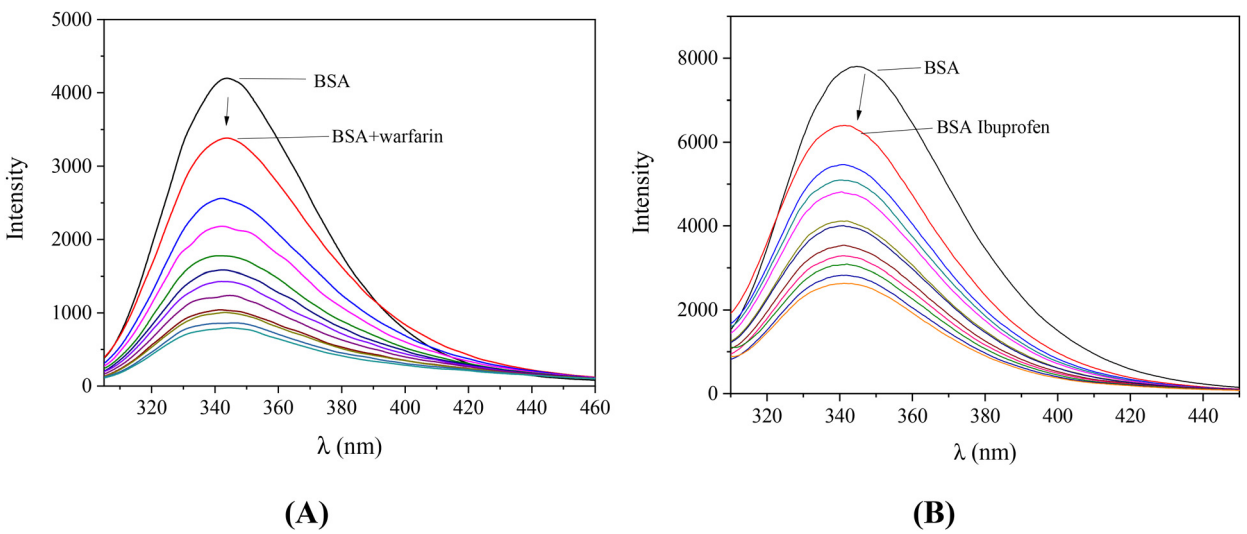


**Fig. 12** Fluorescence emission spectra ($\lambda_{exc}$ = 295 nm) of BSA (3 μM) in a buffer solution (150 mM NaCl and 15 mM sodium citrate, pH 7.0) in the presence of (A) warfarin (3 μM) recorded upon the gradual addition of compound **2**, and (B) ibuprofen (3 μM) recorded upon the incremental addition of compound **3**. The arrows illustrate the intensity changes upon addition of the complexes.

binding site.[31,90] The binding constants of complexes **1** and **2** show a significant decrease in the presence of ibuprofen, suggesting that their primary binding site on BSA is Sudlow site II in subdomain IIIA. For complex **3**, the binding constants to BSA decrease in the presence of both site-markers, with the largest lowering observed in the presence of ibuprofen. This

 

indicates that this complex can bind to both sites, showing a preference for Sudlow site II.

## 4 Conclusions

Four novel hybrid Cu(II) complexes with the quinazoline (*E*)-4-(2-((pyridin-2-yl)methylene)hydrazinyl)quinazoline (HL) or its *in situ* generated methoxylated derivative ($HL^1$) were synthesized in the presence of the NSAIDs Hmef, Hfluf, Hdifl or Na dicl. The resultant complexes $\{[Cu(HL^1)(\mu\text{-}Cl)](difl)\}_n$, $[Cu(L)(mef)(CH_3OH)]\cdot CH_3OH$, $[Cu(L)(dicl)]_n$ and $[Cu_4(L^1)_2(fluf)_4(Cl)_2]\cdot 2H_2O$ were characterized using spectroscopic techniques and single-crystal X-ray crystallography. The biological properties of the complexes were also evaluated with regard to their *in vitro* interaction with BSA and DNA and their antioxidant potency.

In these complexes, the quinazoline ligands exhibited some structural features for the first time: their deprotonation at N2 of the quinazoline ligand (in complexes **2**–**4**) and a tetradentate coordination mode. More specifically, in complexes **1** and **2**, the quinazoline ligands are coordinated in a tridentate fashion, as previously reported complexes of HL or its halogenated derivatives.[31–34] In complexes **3** and **4**, the deprotonated quinazoline ligands are coordinated in a tetradentate bridging mode, which is reported for the first time.

The complexes seem to interact with CT DNA *via* intercalation and the highest DNA-binding constant was found for complex **1** ($K_b$ = 1.80(± 0.01) × $10^7$ $M^{-1}$). The ability of the complexes to cleave plasmid DNA to relaxed circular DNA was high and dependent on the concentration and light used for irradiation. Complex **3** is the most active among the compounds tested, since its high activity was observed at a lower concentration (200 μM) than the other complexes (500 μM). Furthermore, complexes **1**, **2** and **3** showed their highest activity after exposure to visible light, UVA and UVB radiation, respectively.

The ability of the complexes to scavenge DPPH and ABTS free radicals and to reduce $H_2O_2$ was explored within the context of antioxidant activity investigation. Although the complexes were practically inactive towards DPPH radicals, they presented notable scavenging activity towards ABTS radicals, albeit lower than that of the corresponding reference compound Trolox. All complexes were found to be more active towards $H_2O_2$ than the reference compound L-ascorbic acid, with complex **3** being the most active ($H_2O_2$% = 90.11 ± 0.30%) among the compounds.

The binding of the complexes to BSA was found to be tight and reversible, indicating their transport and release at potential biotargets. Competitive studies with the typical site-markers warfarin and ibuprofen revealed the preferable binding of most complexes at Sudlow's site II in subdomain IIIA.

In conclusion, the hybrid Cu(II) complexes reported herein present significantly high (photo)cleavage activity of plasmid DNA and high affinity for CT DNA, which, accompanied by the antioxidant activity and the tight and reversible binding to BSA, make them potential candidates to target DNA.

## Abbreviations

| | |
|---|---|
| ABTS | 2,2′-Azino-bis-(3-ethylbenzothiazoline-6-sulfonic acid) |
| BHT | Butylated hydroxytoluene |
| BSA | Bovine serum albumin |
| CT | Calf-thymus |
| $dicl^{-1}$ | Anion of diclofenac |
| $difl^{-1}$ | Anion of diflunisal |
| DPPH | 1,1-Diphenyl-picrylhydrazyl |
| EB | Ethidium bromide |
| $fluf^{-1}$ | Flufenamato anion |
| Hdicl | Diclofenac |
| Hdifl | Diflunisal |
| Hfluf | Flufenamic acid |
| HL | (*E*)-4-(2-((Pyridin-2-yl)methylene)hydrazinyl) quinazoline |
| $HL^1$ | The methoxylated derivative of HL |
| Hmef | Mefenamic acid |
| $K$ | BSA-binding constant |
| $K_b$ | DNA-binding constant |
| $K_q$ | Quenching constant |
| $K_{SV}$ | Stern–Volmer constant |
| $mef^{-1}$ | Mefenamato anion |
| NDGA | Nordihydroguaiaretic acid |
| NSAID | Non-steroidal anti-inflammatory drug |
| pDNA | pBR322 plasmid DNA |
| Trolox | 6-Hydroxy-2,5,7,8-tetramethylchromane-2-carboxylic acid |
| $\Delta\nu$(COO) | $\nu_{asym}$(COO) − $\nu_{sym}$(COO) |
| $\tau_5$ | Trigonality index |

## Author contributions

Chrisoula Kakoulidou: writing – original draft, methodology, investigation, and formal analysis. Antonios G. Hatizdimitriou: writing – original draft, methodology, and investigation. George Psomas: writing – original draft, writing – review & editing, supervision, project administration, investigation, and conceptualization.

## Data availability

The data supporting this article have been included as part of the ESI.†

CCDC deposition numbers 2418543–2418546 contain the supplementary crystallographic data for the complexes.†

## Conflicts of interest

There are no conflicts to declare.

## References


1 P. Chellan and P. J. Sadler, *Philos. Trans. R. Soc., A*, 2015, **373**, 2014018.
2 M. Jarosz, M. Olbert, G. Wyszogrodzka, K. Młyniec and T. Librowski, *Inflammopharmacology*, 2017, **25**, 11–24.
3 W. X. Tian, S. Yu, M. Ibrahim, A. W. Almonaofy, L. He, Q. Hui, Z. Bo, B. Li and G. L. Xie, *J. Microbiol.*, 2012, **50**, 586–593.
4 S. Medici, M. Peana, V. M. Nurchi, J. I. Lachowicz, G. Crisponi and M. A. Zoroddu, *Coord. Chem. Rev.*, 2015, **284**, 329–350.
5 A. Rivero-Müller, A. De Vizcaya-Ruiz, N. Plant, L. Ruiz and M. Dobrota, *Chem.-Biol. Interact.*, 2007, **165**, 189–199.
6 B. Chudzik, I. B. Tracz, G. Czernel, M. J. Fiolka, G. Borsuk and M. Gagos, *Eur. J. Pharm. Sci.*, 2013, **49**, 850–857.
7 J. Nagaj, R. Starosta and M. Jezowska-Bojczuk, *J. Inorg. Biochem.*, 2015, **142**, 68–74.
8 E. G. Geromichalou, D. T. Trafalis, P. Dalezis, G. Malis, G. Psomas and G. D. Geromichalos, *J. Inorg. Biochem.*, 2022, **231**, 111805.
9 W. Liu, Q. Li, J. Hu, H. Wang, F. Xu and Q. Bian, *Bioorg. Med. Chem.*, 2019, **27**, 115150.
10 S. Ravez, O. Castillo-Aguilera, P. Depreux and L. Goossens, *Expert Opin. Ther. Pat.*, 2015, **25**, 789–804.
11 K. S. van Horn, W. N. Burda, R. Fleeman, L. N. Shaw and R. Manetsch, *J. Med. Chem.*, 2014, **57**, 3075–3093.
12 V. G. Ugale and S. B. Bari, *Eur. J. Med. Chem.*, 2014, **80**, 447–501.
13 X. Su and I. Aprahamian, *Chem. Soc. Rev.*, 2014, **43**, 1963–1981.
14 M. M. E. Shakdofa, M. H. Shtaiwi, N. Morsy and T. M. A. Abdel-Rassel, *Main Group Chem.*, 2014, **13**, 187–218.
15 L. Popiolek, *Med. Chem. Res.*, 2017, **26**, 287–301.
16 S. Rollas and S. G. Kucukgczel, *Molecules*, 2007, **12**, 1910–1939.
17 A. E. Kummerle, M. Schmitt, S. V. S. Cardozo, C. Lugnier, P. Villa, A. B. Lopes, N. C. Romeiro, H. Justiniano, M. A. Martins, C. A. M. Fraga, J. J. Bourguignon and E. J. Barreiro, *J. Med. Chem.*, 2012, **55**, 7525–7545.
18 H. Yamada, A. Shirai, K. Kato, J. Kimura, H. Ichiba, T. Yajima and T. Fukushima, *Chem. Pharm. Bull.*, 2010, **58**, 875–878.
19 T. V. Trashakhova, E. V. Nosova, P. A. Slepukhin, M. S. Valova, G. N. Lipunova and V. N. Charushin, *Russ. Chem. Bull.*, 2011, **60**, 2347–2353.
20 C. N. Banti and S. K. Hadjikakou, *Eur. J. Inorg. Chem.*, 2016, 3048–3071.
21 G. Psomas, *Coord. Chem. Rev.*, 2020, **412**, 213259.
22 K. S. Kim, J. H. Yoon, J. K. Kim, S. J. Baek, T. E. Eling, W. J. Lee, J. H. Ryu, J. G. Lee, J. H. Lee and J. B. Yoo, *Biochem. Biophys. Res. Commun.*, 2004, **325**, 1298–1303.
23 D. H. Woo, I. S. Han and G. Jung, *Life Sci.*, 2004, **75**, 2439–2449.
24 A. Inoue, S. Muranaka, H. Fujita, T. Kanno, H. Tamai and K. Utsumi, *Free Radicals Biol. Med.*, 2004, **37**, 1290–1299.
25 M. T. Kelleni, *Biomed. Pharmacother.*, 2021, **133**, 110982.
26 T. Pringsheim, W. J. Davenport and D. Dodick, *Neurology*, 2008, **70**, 1555–1563.
27 R. S. Vardanyan and V. J. Hruby, in *Synthesis of Essential Drugs*, Elsevier, 2006, pp. 19–55.
28 W. J. Wechter, E. D. Murray, D. Kantoci, D. D. Quiggle, D. D. Leipold, K. M. Gibson and J. D. McCracken, *Life Sci.*, 2000, **66**, 745–753.
29 G. M. Lawton and P. J. Chapman, *Aust. Dent. J.*, 1993, **38**, 265–271.
30 G. Lohrmann, A. Pipilas, R. Mussinelli, D. M. Gopal, J. L. Berk, L. H. Connors, N. Vellanki, J. Hellawell, O. K. Siddiqi, J. Fox, M. S. Maurer and F. L. Ruberg, *J. Card. Failure*, 2020, **26**, 753–759.
31 C. Kakoulidou, P. S. Gritzapis, A. G. Hatzidimitriou, K. C. Fylaktakidou and G. Psomas, *J. Inorg. Biochem.*, 2020, **211**, 111194.
32 C. Kakoulidou, V. R. Kosmas, A. G. Hatzidimitriou, K. C. Fylaktakidou and G. Psomas, *J. Inorg. Biochem.*, 2021, **219**, 111448.
33 C. Kakoulidou, A. G. Hatzidimitriou, K. C. Fylaktakidou and G. Psomas, *Polyhedron*, 2021, **195**, 114986.
34 C. Kakoulidou, C. T. Chasapis, A. G. Hatzidimitriou, K. C. Fylaktakidou and G. Psomas, *Dalton Trans.*, 2022, **51**, 16688–16705.
35 C. Tolia, A. N. Papadopoulos, C. P. Raptopoulou, V. Psycharis, C. Garino, L. Salassa and G. Psomas, *J. Inorg. Biochem.*, 2013, **123**, 53–65.
36 G. Malis, A. S. Bakali, A. G. Hatzidimitriou and G. Psomas, *J. Mol. Struct.*, 2024, **1303**, 137590.
37 F. Dimiza, F. Perdih, V. Tangoulis, I. Turel, D. P. Kessissoglou and G. Psomas, *J. Inorg. Biochem.*, 2011, **105**, 476–489.
38 A. Tarushi, C. P. Raptopoulou, V. Psycharis, C. K. Kontos, D. P. Kessissoglou, A. Scorilas, V. Tangoulis and G. Psomas, *Eur. J. Inorg. Chem.*, 2016, **2016**, 219–231.
39 F. Dimiza, S. Fountoulaki, A. N. Papadopoulos, C. A. Kontogiorgis, V. Tangoulis, C. P. Raptopoulou, V. Psycharis, A. Terzis, D. P. Kessissoglou and G. Psomas, *Dalton Trans.*, 2011, **40**, 8555–8568.
40 S. Fountoulaki, F. Perdih, I. Turel, D. P. Kessissoglou and G. Psomas, *J. Inorg. Biochem.*, 2011, **105**, 1645–1655.
41 J. Marmur, *J. Mol. Biol.*, 1961, **3**, 208–218.
42 M. E. Reichmann, S. A. Rice, C. A. Thomas and P. Doty, *J. Am. Chem. Soc.*, 1954, **76**, 3047–3053.
43 Bruker Analytical X-ray Systems Inc. Apex2 Version 2 User Manual M86-E01078, 2006, preprint.
44 Siemens Industrial Automation Inc. SADABS Area-Detector Absorption Correction, 1996, preprint.
45 L. Palatinus and G. Chapuis, *J. Appl. Crystallogr.*, 2007, **40**, 786–790.
46 P. W. Betteridge, J. R. Carruthers, R. I. Cooper, K. Prout and D. J. Watkin, *J. Appl. Crystallogr.*, 2003, **36**, 1487–1487.
47 C. Lee and R. Matunas, *Compr. Organomet. Chem. III*, 2007, **10**, 649–693.
48 V. Murphy, *Compr. Organomet. Chem. III*, 2007, **1**, 341–379.
49 D. Baba and T. Fuchigami, *Tetrahedron Lett.*, 2003, **44**, 3133–3136.

50 M. F. Yang, X. Yao, L. M. Chen, J. Y. Gu, Z. H. Yang, H. F. Chen, X. Zheng and Z. T. Zheng, *Arch. Pharm.*, 2020, **353**, 2000044.
51 W. J. Geary, *Coord. Chem. Rev.*, 1971, **7**, 81–122.
52 K. Nakamoto, Infrared and Raman Spectra of Inorganic and Coordination Compounds: Part B, in *Applications in Coordination, Organometallic, and Bioinorganic Chemistry*, 2008, pp. 1–408.
53 B. J. Hathaway, in *Comprehensive Coordination Chemistry*, ed. G. Wilkinson, Pergamon Press, Oxford, UK, 1987, vol. 5, pp. 533–773.
54 C. Kutal, *Coord. Chem. Rev.*, 1990, **99**, 213–252.
55 A. W. Addison, T. N. Rao, J. Reedijk, J. Van Rijn and G. C. Verschoor, *J. Chem. Soc., Dalton Trans.*, 1984, 1349–1356.
56 P. K. Tsobnang, E. Hasturk, D. Frohlich, E. Wenger, P. Durand, J. L. Ngolui, C. Lecomte and C. Janiak, *Cryst. Growth Des.*, 2019, **19**, 2869–2880.
57 J. Pitarch-Jarque, H. R. Jiménez, E. Kalenius, S. Blasco, A. Lopera, M. P. Clares, K. Rissanen and E. García-España, *Dalton Trans.*, 2021, **50**, 9010–9015.
58 R. Cortes, L. Lezama, J. I. R. de Larramendi, G. Madariaga, J. L. Mesa, F. J. Zuniga and T. Rojo, *Inorg. Chem.*, 1995, **34**, 778–786.
59 R. Singh, F. Lloret and R. Mukherjee, *Z. Anorg. Allg. Chem.*, 2014, **640**, 1086–1094.
60 X. H. Bu, M. Du, Z. L. Shang, R. H. Zhang, D. Z. Liao, M. Shionoya and T. Clifford, *Inorg. Chem.*, 2000, **39**, 4190–4199.
61 X. J. Zhao, M. Du, Y. Wang, J. H. Guo and X. H. Bu, *Inorg. Chim. Acta*, 2005, **358**, 4481–4488.
62 H. Gao, M. M. Liu, Q. G. Zhai, X. X. Wei, J. X. Yang and X. M. Zhang, *J. Solid State Chem.*, 2019, **276**, 244–250.
63 C. C. Hsieh, P. K. Liao, C. W. Chen, M. H. Chiang and Y. C. Horng, *Dalton Trans.*, 2023, **52**, 4429–4441.
64 K. Choroba, B. Machura, K. Erfurt, A. R. Casimiro, S. Cordeiro, P. V. Baptista and A. R. Fernandes, *J. Med. Chem.*, 2024, **67**, 5813–5836.
65 M. Du, Y. M. Guo, X. H. Bu, J. Ribas and M. Monfort, *New J. Chem.*, 2002, **26**, 939–945.
66 A. R. Battle, B. Graham, L. Spiccia, B. Moubaraki, K. S. Murray, B. W. Skelton and A. H. White, *Inorg. Chim. Acta*, 2006, **359**, 289–297.
67 A. Barmpa, A. G. Hatzidimitriou and G. Psomas, *J. Inorg. Biochem.*, 2021, **217**, 111357.
68 M. Lazou, A. G. Hatzidimitriou, A. N. Papadopoulos and G. Psomas, *J. Inorg. Biochem.*, 2023, **243**, 112196.
69 L. P. Battaglia, A. B. Corradi, G. Marcotrigiano, L. Menabue and G. C. Pellacani, *Inorg. Chem.*, 1979, **18**, 148–152.
70 L. Yang, D. R. Powell and R. P. Houser, *Dalton Trans.*, 2007, 955–964.
71 A. Okuniewski, D. Rosiak, J. Chojnacki and B. Becker, *Polyhedron*, 2015, **90**, 47–57.
72 A. Wolfe, G. H. Shimer and T. Meehan, *Biochemistry*, 1987, **26**, 6392–6396.
73 A. Dimitrakopoulou, C. Dendrinou-Samara, A. A. Pantazaki, M. Alexiou, E. Nordlander and D. P. Kessissoglou, *J. Inorg. Biochem.*, 2008, **102**, 618–628.
74 A. M. Pizarro and P. J. Sadler, *Biochimie*, 2009, **91**, 1198–1211.
75 B. J. Pages, D. L. Ang, E. P. Wright and J. R. Aldrich-Wright, *Dalton Trans.*, 2015, **44**, 3505–3526.
76 J. R. Lakowicz, Principles of fluorescence spectroscopy, Springer, 2006.
77 D. P. Heller and C. L. Greenstock, *Biophys. Chem.*, 1994, **50**, 305–312.
78 M. M. Gineinah, M. A. El-Sherbeny, M. N. Nasr and A. R. Maarouf, *Arch. Pharm.*, 2002, **335**, 556–562.
79 A. M. Alafeefy, A. A. Kadi, O. A. Al-Deeb, K. E. H. El-Tahir and N. A. Al-Jaber, *Eur. J. Med. Chem.*, 2010, **45**, 4947–4952.
80 C. Kontogiorgis, M. Ntella, L. Mpompou, F. Karallaki, P. Athanasios, D. Hadjipavlou-Litina and D. Lazari, *J. Enzyme Inhib. Med. Chem.*, 2016, **31**, 154–159.
81 S. Dairi, M. A. Carbonneau, T. Galeano-Diaz, H. Remini, F. Dahmoune, O. Aoun, A. Belbahi, C. Lauret, J. P. Cristol and K. Madani, *Food Chem.*, 2017, **237**, 297–304.
82 B. M. Ali, M. Boothapandi and A. S. S. Nasar, *Data Brief*, 2020, **28**, 104972.
83 S. Perontsis, A. G. Hatzidimitriou and G. Psomas, *Dalton Trans.*, 2024, **53**, 15215–15235.
84 M. Wettasinghe and F. Shahidi, *Food Chem.*, 2000, **70**, 17–26.
85 R. E. Olson and D. D. Christ, *Annu. Rep. Med. Chem.*, 1996, **31**, 327–336.
86 L. Stella, A. L. Capodilupo and M. Bietti, *Chem. Commun.*, 2008, 4744–4746.
87 Y.-Q. Wang, H.-M. Zhang, G.-C. Zhang, W.-H. Tao and S.-H. Tang, *J. Lumin.*, 2007, **126**, 211–218.
88 O. H. Laitinen, V. P. Hytönen, H. R. Nordlund and M. S. Kulomaa, *Cell. Mol. Life Sci.*, 2006, **63**, 2992–3017.
89 G. Sudlow, D. J. Birkett and D. N. Wade, *Mol. Pharmacol.*, 1976, **12**, 1052–1061.
90 M. Lazou, A. Tarushi, P. Gritzapis and G. Psomas, *J. Inorg. Biochem.*, 2020, **206**, 111019.